

The phase curve survey of the irregular saturnian satellites: A possible method of physical classification

James M. Bauer^{a,*}, Tommy Grav^b, Bonnie J. Buratti^a, Michael D. Hicks^a

^a *Jet Propulsion Laboratory, Palomar Observatory, California Institute of Technology, 4800 Oak Grove Drive, Mailstop 183-501, Pasadena, CA 91109, USA*

^b *Institute for Astronomy, University of Hawaii, 2860 Woodlawn Drive, Honolulu, HI 96822, USA*

Received 2 November 2005; revised 11 April 2006

Available online 12 June 2006

Abstract

During its 2005 January opposition, the saturnian system could be viewed at an unusually low phase angle. We surveyed a subset of Saturn's irregular satellites to obtain their true opposition magnitudes, or nearly so, down to phase angle values of 0.01° . Combining our data taken at the Palomar 200-inch and Cerro Tololo Inter-American Observatory's 4-m Blanco telescope with those in the literature, we present the first phase curves for nearly half the irregular satellites originally reported by Gladman et al. [2001. *Nature* 412, 163–166], including Paaliaq (SXX), Siarnaq (SXXIX), Tarvos (SXXI), Ijiraq (SXXII), Albiorix (SXVI), and additionally Phoebe's narrowest angle brightness measured to date. We find centaur-like steepness in the phase curves or opposition surges in most cases with the notable exception of three, Albiorix and Tarvos, which are suspected to be of similar origin based on dynamical arguments, and Siarnaq.

© 2006 Elsevier Inc. All rights reserved.

Keywords: Saturn, satellites; Satellites, surfaces; Photometry

1. Introduction

The irregular satellites of Saturn include those that have high inclination and eccentric orbits; additionally they have large semi-major axes relative to the regular satellites. In light of these dynamical characteristics, these irregular satellites are believed to be captured bodies, not formed within Saturn's protoplanetary disk, but rather in more distant regions of the pre-solar nebula and later perturbed into orbits about the saturnian system (Gladman et al., 2001). With the exception of Phoebe, which was discovered in 1899 (cf. Pickering, 1899), the saturnian irregular satellites have been recently discovered, since 2000, and the brightest among these newest irregulars, Siarnaq (SXXIX), is 20th mag (R band). Hence most of these bodies are difficult to characterize with even meter-sized telescopes. Nonetheless, several associations or groupings among the saturnian irregular satellites have been proposed based on their observed dynamical (Gladman et al., 2001; Cuk and Burns, 2004)

and broad-band color (Grav et al., 2003; Grav and Holman, 2004) properties. Additionally, there have been several theorized relations to other outer Solar System populations, such as the comets, centaurs, and KBOs, based on spectral–photometric (Grav and Holman, 2004; Buratti et al., 2005a), photometric (Bauer et al., 2004), and spectroscopic (Owen et al., 1999; Brown, 2000; Buratti et al., 2002; Clark et al., 2005) evidence, as well as density constraints (Johnson and Lunine, 2005). An accurate interpretation of the link to such minor body populations is critical to our understanding of the mechanisms of volatile transport from the outer to the inner Solar System. Volatiles in the inner Solar System, including H_2O , are believed to originate in part from comets. The ultimate source of these cometary bodies and volatiles is in the outer Solar System, specifically the Kuiper belt and Oort cloud (Luu, 1994; Durda and Stern, 2000), where volatiles may survive since from the time of Solar System formation. These inbound cometary bodies must pass through the regions between the giant planets (e.g., Horner et al., 2004), and tracing their intermediary path is key to understanding the details of the transport process.

In order to test these relationships, and to sample the phase curves of these outer Solar System bodies, we observed these ir-

* Corresponding author. Fax: +1 818 393 4445.

E-mail address: bauer@scn.jpl.nasa.gov (J.M. Bauer).

regular satellites during Saturn’s January 2005 opposition. This opposition event was a unique opportunity to study the saturnian system in that it afforded a rare low phase-angle (α) viewing, down to a few hundredths of a degree (Verbiscer et al., 2005a); these were circumstances that would not be repeated for over four decades. If viewed from Saturn, or the irregular satellites Phoebe and Ymir, the Earth would have transited the Sun during this rare opposition. Near the very narrowest of phase angles, as α approaches its minimum (α_{\min}), the Sun’s finite size begins to play a significant role in determining the shape of a body’s phase curve. At angles on the order of the Sun’s angular radius at the body’s heliocentric distance (α_R) the phase curve is essentially blunted. Here the phase curve flattens for angles significantly less than α_R , as observed for the case of the Moon by the Clementine mission (Buratti et al., 1996). Our planned coverage of Ymir ($\alpha_{\min} \approx 0.01^\circ$, during the 2005 opposition) and Phoebe ($\alpha_{\min} \approx 0.02$) would reach this “turnover regime,” where $\alpha_{\min} \leq \alpha_R$ ($\approx 0.029^\circ$). For Phoebe, owing to approaching twilight, we were able to obtain data down to $\alpha = 0.028^\circ$, less than α_R by only about 4%, and so the phase “turnover” effect could not have been very strong at this point. However, for similar geometries with the Clementine data (Buratti et al., 1996), the brightness value at $\alpha = 0.96\alpha_R$ was less than 0.02 magnitudes from its α_{\min} value, which is within the uncertainty of absolute photometry for most ground based telescopes’ data points of this saturnian moon.

By comparison to the phase curves of other outer Solar System bodies, one may identify possible links with minor planet or comet populations. The centaurs, for example, have been reported to have unusually steep phase curves (cf. Elatus, Bauer et al., 2002; Pelion, Bauer et al., 2003; and 2000 EC98, Rousselot et al., 2005) with some G -parameter values of <0 . Members of the trans-neptunian populations have varied phase curve responses ranging from similarly steep, with reported negative IAU model G -parameters (Sheppard and Jewitt, 2002) to the more shallow (cf. Pluto, with $G \approx 0.8$; Tholen and Tedesco, 1994) with G -parameter values ≥ 0.2 . Generally, an object will appear to brighten as it is viewed from narrower viewing phase angles. At angles of several tens to several degrees, the brightening is primarily owing to an object’s surface roughness on scales greater than a few centimeters, as the shadows that the larger surface features cast become hidden from view (cf. Seeliger, 1895; Buratti and Veverka, 1985; Hapke, 1993). The phase response at angles smaller than $\sim 5^\circ$ is referred to as the opposition surge. This portion of the phase curve holds specific information regarding the particle size and filling factors, or the surficial compaction, on centimeter scales or smaller (Buratti et al., 1996), which may be attributed to particle shadow hiding effects (Irvine, 1965; Hapke, 1993). These phenomena dominate the opposition surge when, for example, the reflectivity of the surface material is low, so that the photons will be absorbed after multiple scatterings and the reflected light does not have a chance to brighten the shaded regions (Shkuratov and Helfenstein, 2001). Phenomena with large multiple scattering components, such as coherent back-scattering (CBS; Hapke, 2002) may contribute to the opposition surge as well. Originally proposed to ex-

plain the opposition surges on multiply scattering, high albedo surfaces (Oetking, 1966), but later shown to have a single-scattering component as well (Helfenstein et al., 1997), CBS is an effect caused by constructive interference between wave fronts from light scattered off different surfaces, but traveling along the same pathways in opposite directions (Ozrin, 1992; Hapke, 1993; Nelson et al., 2000), and may contribute at very narrow phase angles of $\leq 0.5^\circ$, to the opposition surge. However, as these two different effects driving the opposition surge respond differently to the ratio of the mean particle size to the observation wavelength, and lighter ($p > 0.15$) or darker ($p < 0.15$) reflectance (Shkuratov and Helfenstein, 2001), it may be possible, at least on darker surfaces, to distinguish between the two by sampling the narrow angle phase curves at separate wavelengths, where the reflectance may differ. Specifically, CBS theory predicts a strengthening of the opposition surge at longer wavelengths (Hapke, 1993). Considering that many of the irregular satellite surfaces are neutral or red, CBS should further exhibit a secondary increase to the opposition surge at longer wavelengths owing to the fact that the surface albedos increase toward moderate values, whereas shadow hiding should show a diminished surge as multiply scattered photons partly illuminate primary shadows.

2. Observations

The saturnian system went through its 2005 opposition on the nights of January 13 and 14 UT. The irregular satellites achieved minimum viewing phase from Earth at different times over the two nights. The orbits of these moons extend many tens of arcminutes over Saturn’s field of view. In order to obtain data for as many satellites as possible, and to cover as wide a range of phase angles as possible, we proposed for time on both the Palomar 200-inch and the Cerro Tololo (CTIO) Blanco 4-m telescopes, using wide field mosaic cameras to image multiple satellites for many of the exposures. Our extended coverage also allowed us to monitor for potential variation owing to rotational light curve signal. The Palomar Observatory’s Large Format Camera (LFC) is a 6-chip $2k \times 4k$ mosaic array, with a 24 arcmin FOV (maximum extent) on a side. The CTIO MOSAIC-2 camera is an 8-chip $2k \times 4k$ mosaic array, with a 36 arcmin FOV on a side. We operated both cameras in 2×2 binning mode, with a 0.36 arcsec/pixel plate scale for the LFC and a 0.54 arcsec/pixel plate scale for the MOSAIC-2, to conserve data storage space and minimize readout time. The seeing exceeded the plate scale by at least a factor of 2 in both instances. We observed in two filters, B and R bands, at both telescopes. We chose these two filter passes in consideration of the wavelength baseline separation, to detect any differences in the opposition surges based on wavelength, along with the detector responses and expected signal-to-noise (S/N) levels of our objects at both telescopes. Each chip was calibrated with Landolt (1992) standard field stars, taken at multiple airmasses, for zero point offsets, color terms, and extinction coefficients. Using IRAF (Tody, 1986) to flatten and bias subtract the images, cosmic ray elimination was conducted “by hand,” by individually replacing affected pixels with the average of the adjoining pix-

Table 1
Observational circumstances

Dates (UT)	Location	Instrument	Pixel scale ^a	FOV ^b	Seeing ^c	Transparency
January 13, 5.0–8.1	CTIO	MOSAIC-2	0.54	24	1.5	Mostly clear, thin cirrus at 9 UT
January 13, 3–14	Palomar	LFC	0.36	24	2.0	Clear all night
January 14, 1.9–8.1	CTIO	MOSAIC-2	0.54	24	1.5	Variable cirrus throughout night
January 14, 3–14	Palomar	LFC	0.36	24	?	Thick clouds

^a Units of arcsec per pixel.

^b In units of arcmin on a side.

^c Arcsec per FWHM

els. Counts were extracted from the images using an aperture photometry technique, with 5 arcsec aperture diameters.

We were allocated two full nights, January 13 and 14 (UT), on the Palomar 200-inch and the second half-night on the 13th and the full night of the 14th on the CTIO 4-m telescope. The observing conditions are summarized in Table 1. Our first night on the 200-inch was clear, and our second was clouded over. Our half-night on the 4-m was mostly clear, with cirrus arriving around 9 UT, allowing us to still calibrate our exposures. The second night at the 4-m had variable cirrus throughout the night, but we were able to conduct relative photometry on many of our frames using background stars selected in the exposures from the 13th taken at Palomar and CTIO. These background stars were designated as “frame standards” after looking for photometric stability across the night of January 13th and rejecting any that showed signs of variability. After screening for variability, three or more frame standards were selected that overlapped both nights and these were used to compare with each satellite’s signal. The uncertainties from the dispersion in the frame standard magnitude offsets relative to their measured magnitudes from the previous night are folded into the photon statistical uncertainties from the irregular satellites as listed in our measured magnitudes (Table 2). The seeing at Palomar on the night of the 13th was notably poorer than that at CTIO, and so we introduced an offset ~ -0.07 to the LFC magnitudes, based on the differences between our frames standards, in order to align our absolute magnitude values between the two telescope data sets. Scattered light or secondary reflections from Saturn was a problem with several of the exposures, as the fainter objects had lengthy exposures on the order of 600 s. Consequently, some of the frames were rejected on the basis of the extremely high or locally varying background, and were not included in the final reduction.

Our data for the satellites Albiorix and Siarnaq were supplemented by images taken at Table Mountain Observatory’s (TMO) 0.6-m telescope on September 23rd–October 15th of 2004. The other irregular satellites were too faint to observe from TMO. The nights were photometric, and the data were reduced in a similar manner as the Palomar data; the extinction and zero-point corrections were made using Landolt standards (see Bauer et al., 2004 for a description of the reduction techniques specific to TMO data). Exposures were 20 min in length, and the uncertainty in each frame’s magnitude was large, exceeding their measured magnitude variations, and so we used only the average magnitudes, reported in Table 3, in our analysis.

3. Analysis

3.1. Phase curve photometry

The satellites discovered by Gladman et al. (2001) had few actual samplings over a limited range of phase angle values accessible to ground based viewing ($\alpha < 6.4^\circ$). It was not possible, then, to fit more complicated phase models, such as that developed by Hapke (1993), to the data thus far. However, we were able to fit the IAU model, similar to that developed by Lumme and Bowell (Bowell et al., 1989) for the analysis of asteroid phase curves. This model is essentially a fit to only two parameters, zero-phase absolute (Solar-System) magnitude, $H(1, 1, 0)$, and the slope-parameter, G . The shape of the phase curve is fixed by the value of G alone. The IAU model is somewhat heuristic, and so only in as much as several asteroid phase curves sampled in the development of the model may have included finite-solar-size effects does it incorporate such effects at all. The IAU model is certainly not optimal in that it ultimately leads one to a qualitative rather than quantitative interpretation of certain physical parameters, such as the particle filling factor. However, as it has been widely applied and may be fit to a limited phase sampling of a particular object, it does allow for a method of differentiation and comparison between these satellites as well as with other outer Solar System small bodies. We were able to obtain nearly accurate $H_R(1, 1, 0)$ values, as most of our data included points sampled where the phase angle was a few times, or in two cases less than, the solar disk’s angular radius at Saturn’s distance. The results of the fits are summarized in Table 4 and Figs. 1–7. With the exception of Siarnaq and Phoebe, the rotational variations of the irregular satellites are uncharacterized; Siarnaq’s is only partially characterized (Buratti et al., 2005a). For the fitted data values (except for Phoebe’s), uncertainties corresponding to a light curve amplitude identical to Phoebe’s were folded in to the photometric uncertainties of the data points.

3.1.1. Phoebe

Phoebe’s phase curve data and fits are shown in Fig. 1, including data from Bauer et al. (2004), Kruse et al. (1986), and Degewij et al. (1980). In Fig. 1A, the averages of the R- and B-band magnitudes are shown, after the rotational amplitude offsets were removed. The B-band data were shifted in the figure based on colors from the literature (Degewij et al., 1980). The amplitude offsets were estimated from Bauer et al. (2004) using the ephemeris longitudes provided by JPL’s Hori-

Table 2
Observed magnitudes

Time (UT)/date (MJD) ^a	Exp. (s)	α (°) ^b	Filter	$m_{R,B}$ ^c	$H(1, 1, \alpha)$ ^d	σ	Comments
Phoebe [$R = 9.15$, $\Delta = 8.16$] ^e							
January 13 [PA = 280.5°, $\Delta\theta = 1190''$] ^f							
03:38:33/3383.651811	7	0.067	R	15.558	6.192	0.022	
04:40:37/3383.694913	7	0.062	R	15.675	6.309	0.023	
04:43:15/3383.696742	7	0.062	R	15.674	6.308	0.023	
06:12:12/3383.758513	7	0.054	R	15.637	6.271	0.023	
06:22:40/3383.765781	7	0.053	R	15.621	6.255	0.022	
06:45:53/3383.781904	7	0.051	R	15.636	6.270	0.021	
06:51:49/3383.786024	7	0.051	R	15.646	6.280	0.021	
06:53:34/3383.787240	7	0.051	R	15.631	6.265	0.021	
07:54:13/3383.829358	7	0.046	R	15.591	6.225	0.022	
07:59:37/3383.833108	7	0.045	R	15.607	6.241	0.022	
11:13:00/3383.967402	7	0.029	R	15.589	6.223	0.022	
11:14:07/3383.968177	7	0.029	R	15.613	6.247	0.022	
04:23:31/3383.683038	7	0.064	B	16.678	7.312	0.028	
06:24:44/3383.767216	7	0.053	B	16.579	7.213	0.062	
06:27:08/3383.768883	7	0.052	B	16.585	7.219	0.081	
07:56:09/3383.830700	7	0.045	B	16.627	7.261	0.076	
07:57:55/3383.831927	7	0.045	B	16.658	7.292	0.094	
11:19:17/3383.971765	7	0.028	B	16.659	7.293	0.027	
11:20:32/3383.972633	7	0.028	B	16.564	7.198	0.027	
January 14 [PA = 280.3°, $\Delta\theta = 1205''$]							
01:54:47/3384.579751	7	0.044	R	15.643	6.277	0.032	
02:04:45/3384.586979	60	0.044	R	15.637	6.271	0.068	Thickening cirrus
02:27:22/3384.602454	20	0.046	R	15.659	6.294	0.032	Thickening cirrus
02:37:48/3384.609670	15	0.047	R	15.705	6.339	0.038	Thickening cirrus
02:40:55/3384.611834	15	0.047	R	15.681	6.315	0.028	Thickening cirrus
04:25:41/3384.684531	7	0.056	R	15.637	6.272	0.031	
04:31:26/3384.688536	7	0.057	R	15.641	6.275	0.022	
06:22:24/3384.765596	7	0.066	R	15.585	6.219	0.022	
07:42:40/3384.821337	7	0.073	R	15.575	6.210	0.024	
07:45:26/3384.823258	7	0.073	R	15.589	6.224	0.027	
02:30:31/3384.604641	20	0.046	B	16.617	7.252	0.022	Thickening cirrus
02:33:45/3384.606887	20	0.047	B	16.564	7.198	0.027	Thickening cirrus
04:28:36/3384.686568	7	0.056	B	16.551	7.185	0.021	
04:30:00/3384.687888	7	0.057	B	16.606	7.241	0.020	
06:19:37/3384.763663	7	0.065	B	16.550	7.184	0.020	
07:44:00/3384.822263	7	0.060	B	16.559	7.194	0.024	
Ymir [$R = 9.16$, $\Delta = 8.18$]							
January 13 [PA = 78.4°, $\Delta\theta = 968''$]							
07:24:23/3383.810336	300	0.111	R	21.101	11.845	0.073	
07:31:33/3383.815313	300	0.110	R	21.046	11.800	0.077	
January 14 [PA=77.9°, $\Delta\theta = 953''$]							
08:02:13/3384.836609	300	0.012	R	21.102	11.736	0.114	
Paaliaq [$R = 9.10$, $\Delta = 8.12$]							
January 13 [PA = 323.9°, $\Delta\theta = 3469''$]							
07:40:01/3383.821192	300	0.073	R	20.597	11.254	0.041	
07:47:00/3383.826042	300	0.073	R	20.521	11.178	0.038	
08:42:33/3383.864618	300	0.076	R	20.705	11.362	0.037	
08:50:53/3383.870405	300	0.076	R	20.705	11.363	0.037	
09:08:11/3383.882419	300	0.056	B	21.866	12.523	0.076	
January 14 [PA = 324.0°, $\Delta\theta = 3464''$]							
03:42:21/3384.656146	300	0.117	R	20.635	11.294	0.052	
05:21:54/3384.725278	300	0.124	R	20.470	11.127	0.082	
07:20:33/3384.807674	300	0.132	R	20.484	11.142	0.083	
03:50:00/3384.661458	300	0.090	B	21.895	12.552	0.118	
07:26:48/3384.812014	300	0.110	B	22.018	12.675	0.133	

(continued on next page)

Table 2 (continued)

Time (UT)/date (MJD) ^a	Exp. (s)	α ($^{\circ}$) ^b	Filter	$m_{R,B}$ ^c	$H(1, 1, \alpha)$ ^d	σ	Comments
Sirmaq [$R = 8.94$, $\Delta = 7.96$]							
January 13 [PA = 210.8 $^{\circ}$, $\Delta\theta = 3405''$]							
03:44:25/3383.656539	120	0.118	R	19.424	10.163	0.028	
03:48:33/3383.659410	120	0.118	R	19.495	10.234	0.029	
06:32:26/3383.773218	120	0.110	R	19.552	10.291	0.034	
06:48:28/3383.784352	120	0.109	R	19.5047	10.242	0.034	
03:53:55/3383.663137	120	0.117	B	20.810	11.549	0.063	
03:58:57/3383.666632	120	0.117	B	20.832	11.570	0.065	
04:04:52/3383.670741	120	0.116	B	20.933	11.672	0.047	
04:11:44/3383.675509	120	0.116	B	20.851	11.590	0.055	
06:42:57/3383.780521	120	0.109	B	20.800	11.538	0.049	
January 14 [PA = 211.0 $^{\circ}$, $\Delta\theta = 3409''$]							
02:44:21/3384.614826	120	0.108	R	19.582	10.321	0.033	
02:50:48/3384.619306	120	0.109	R	19.567	10.305	0.044	
04:34:05/3384.691030	120	0.113	R	19.466	10.205	0.026	
04:41:27/3384.696146	120	0.113	R	19.513	10.251	0.028	
06:24:47/3384.768252	180	0.118	R	19.584	10.322	0.025	Cirrus
06:40:11/3384.778947	180	0.118	R	19.554	10.293	0.042	Cirrus
07:47:17/3384.824850	60	0.121	R	19.506	10.245	0.034	
07:51:49/3384.827998	60	0.122	R	19.550	10.289	0.033	
02:54:18/3384.621736	120	0.109	B	20.927	11.666	0.063	
02:57:28/3384.623935	120	0.109	B	20.875	11.614	0.054	
04:37:51/3384.693646	120	0.113	B	20.779	11.518	0.054	
07:49:24/3384.826319	60	0.121	B	20.922	11.661	0.081	
Tarvos [$R = 8.99$, $\Delta = 8.01$]							
January 13 [PA = 72.5 $^{\circ}$, $\Delta\theta = 3627''$]							
10:41:34/3383.947269	300	0.174	R	22.283	12.996	0.192	
10:48:03/3383.951655	300	0.173	R	21.840	12.553	0.127	
January 14 [PA = 72.5 $^{\circ}$, $\Delta\theta = 3613''$]							
03:57:31/3384.666678	300	0.095	R	22.130	12.843	0.197	
04:03:42/3384.670972	300	0.095	R	22.049	12.762	0.211	
07:34:33/3384.817396	300	0.080	R	21.984	12.697	0.221	
Ijiraq [$R = 9.00$, $\Delta = 8.01$]							
January 13 [PA = 301.9 $^{\circ}$, $\Delta\theta = 848''$]							
07:14:53/3383.803738	300	0.037	R	22.158	12.869	0.293	
11:05:46/3383.964190	300	0.044	R	21.932	12.643	0.232	
Albiorix [$R = 8.94$, $\Delta = 7.95$]							
January 13 [PA = 238.7 $^{\circ}$, $\Delta\theta = 2844''$]							
06:10:21/3383.757882	120	0.063	R	20.192	10.859	0.025	
06:16:31/3383.762164	120	0.062	R	20.261	10.929	0.026	
06:32:26/3383.773218	120	0.062	R	20.232	10.973	0.038	
06:48:28/3383.784352	120	0.061	R	20.098	10.838	0.035	
07:43:48/3383.822778	120	0.058	R	20.124	10.792	0.023	
04:29:37/3383.687928	120	0.067	B	21.452	12.193	0.022	
04:31:14/3383.689051	120	0.066	B	21.463	12.204	0.022	
06:42:57/3383.780521	120	0.061	B	21.489	12.230	0.093	
07:09:36/3383.799028	120	0.060	B	21.538	12.279	0.057	
07:15:41/3383.803252	120	0.059	B	21.489	12.230	0.056	
07:23:23/3383.808600	120	0.059	B	21.426	12.167	0.041	
January 14 [PA = 238.8 $^{\circ}$, $\Delta\theta = 2857''$]							
02:44:21/3384.614826	120	0.096	R	20.104	10.845	0.052	
02:50:48/3384.619306	120	0.097	R	20.171	10.912	0.071	
04:34:05/3384.691030	120	0.104	R	20.112	10.853	0.038	
04:41:27/3384.696146	120	0.104	R	20.055	10.796	0.040	
06:24:47/3384.767905	120	0.112	R	20.169	10.909	0.035	
06:35:57/3384.775660	180	0.113	R	20.240	10.981	0.353	Cirrus
06:40:11/3384.778600	180	0.113	R	20.075	10.816	0.062	Cirrus
07:47:17/3384.825197	120	0.118	R	20.208	10.949	0.059	
07:51:49/3384.828345	120	0.118	R	20.094	10.835	0.061	

(continued on next page)

Table 2 (continued)

Time (UT)/date (MJD) ^a	Exp. (s)	α (°) ^b	Filter	$m_{R,B}$ ^c	$H(1, 1, \alpha)$ ^d	σ	Comments
02:54:19/3384.621748	120	0.097	B	21.3654	12.106	0.109	
02:57:28/3384.623935	120	0.098	B	21.338	12.079	0.096	
04:37:51/3384.693646	120	0.104	B	21.480	12.221	0.094	
07:49:24/3384.826319	60	0.118	B	21.259	12.000	0.122	

^a UT start time of integration and central integration time in units of JD-2450000.0.

^b Satellite phase angle at the time of observation.

^c Observed R- or B-band magnitude.

^d Magnitude corrected for distance alone, without phase correction.

^e Satellite's heliocentric (R) and observer (Δ) distance in AU.

^f Position angle (PA) from Saturn's center, in degrees, and separation ($\Delta\theta$) from Saturn in units of arcsec. Geometric data obtained from JPL's Horizon's ephemerides service (<http://ssd.jpl.nasa.gov>).

Table 3

TMO observational summary and average magnitudes

Object	Dates (2004)	R	Δ	α	m_R	$H_R(1, 1, \alpha)$	σ	Comments
Albiorix	09/23–10/15	9.15	8.92	6.2	20.65	11.11	0.11	Individual point dispersions were folded into σ
Siarnaq	09/23–10/15	9.13	8.92	6.2	20.23	10.67	0.12	

Table 4

IAU 2-parameter model fits

Object	H_R	H_B	G_R	G_B
Phoebe	6.24 ± 0.009	7.186 ± 0.008	$+0.02 \pm 0.03$	-0.07 ± 0.03
Albiorix	10.86 ± 0.01	12.14 ± 0.04	$+0.39 \pm 0.06$	$+0.33 \pm 0.12$
Tarvos	12.73 ± 0.08	–	$+0.42 \pm 0.24$	–
Siarnaq	10.38 ± 0.04	11.77 ± 0.03	$+0.45 \pm 0.17$	$+0.41 \pm 0.18$
Paaliaq	11.23 ± 0.04	12.54 ± 0.03	$+0.04 \pm 0.12$	-0.13 ± 0.14
Ijiraq	12.73 ± 0.11	–	-0.11 ± 0.17	–

zon's ephemeris service (<http://www.ssd.jpl.nasa.gov>), which was updated using the Bauer et al. (2004) and recent Cassini observations (cf. Clark et al., 2005). The appropriate offsets for each data point were determined from a box-car average of the individual point offsets from the Bauer et al. (2004) light curve within 10° of the longitudes corresponding to the points from the January 2005 data. The individual magnitude points, with the light curve amplitude removed, are shown in Fig. 1B. The model fits were made for the R-band data, with the best fit model indicated by the solid lines and fit uncertainties by dashed and dotted lines. The former model fits, based upon the analysis in Bauer et al. (2004), similar to the Kruse et al. (1986) analysis, are shown as a magenta dot-dashed line. It is clear from the opposition data's location in panels A and B that the opposition surge is stronger than predicted. This finding resulted in a steeper fit (lower G -parameter value, see Bauer et al., 2002) to the data, and a G -value more consistent with those measured for centaur bodies (Bauer et al., 2003; Rousselot et al., 2005). The B-band data, offset to align with the R-band data using Phoebe's B–R colors (Degewij et al., 1980), and indicated by the green data points, show a yet stronger surge at these shorter wavelengths. The literature colors used were derived from color photometry obtained when Phoebe was viewed at phase angles of several degrees. Hence, the B-band data points offset at $\alpha \leq 0.2^\circ$ is caused by a comparatively stronger opposition surge at these shorter wavelengths. This opposition surge strengthening at shorter wavelengths is further

demonstrated by comparison of the R- and B-band fit results shown in Table 4; the IAU model slope parameter is steeper in B ($G = -0.07 \pm 0.03$) by 3 standard deviations from the R-band value ($G = +0.02 \pm 0.03$). No significant brightening trends were apparent for phase values of less than 0.08° .

3.1.2. Albiorix and Tarvos

The irregular satellites we sampled from the 34° inclination group, Albiorix and Tarvos, are shown in Figs. 2 and 3. The averages of the B (offset to align with R using the Grav et al. (2003) colors, which were obtained at higher phase angles than our data's colors) and R-band points are shown in Figs. 2A–7A. No rotational variation was subtracted from the opposition points in B, as the rotation states of any of the Gladman et al. (2001) satellites are not fully characterized. The R-band data values used to fit the IAU phase curve model are indicated as black points. Fig. 2 shows data points from Grav et al. (2003) and Grav (2006; in preparation), which were used to fit the IAU model. The $\alpha = 5.2^\circ$ R-band photometry from Grav (2006; in preparation) was an average over several points, likely spanning the rotational light curve amplitude estimated to be $\sim 0.05m_R$. Individual data points obtained at JPL's Table Mountain Observatory's 0.6-m telescope are also shown along with their average, which was used in the phase curve model fit as well. Discovery data points were not used for Albiorix owing to the relatively large range of values first reported (Gladman and Holman, 2000). The B-band data for Albiorix was also fit with an IAU model, and the results are tabulated in Table 4. As with Siarnaq and Paaliaq, the B-band data fit yielded slightly steeper slope parameters, but not significantly different, from the R-band fits. Only three phase angle data clusters were used to fit the Tarvos phase curve; the data near 6° phase angle were from Grav (2006; in preparation), and at 4.4° were from Grav et al. (2003). The discovery data points are also used in the fits (Gladman et al., 2000a). Our estimate of the error in the discovery data points was on the order of 0.2 magnitudes, as it was unclear whether these values were from completely reduced im-

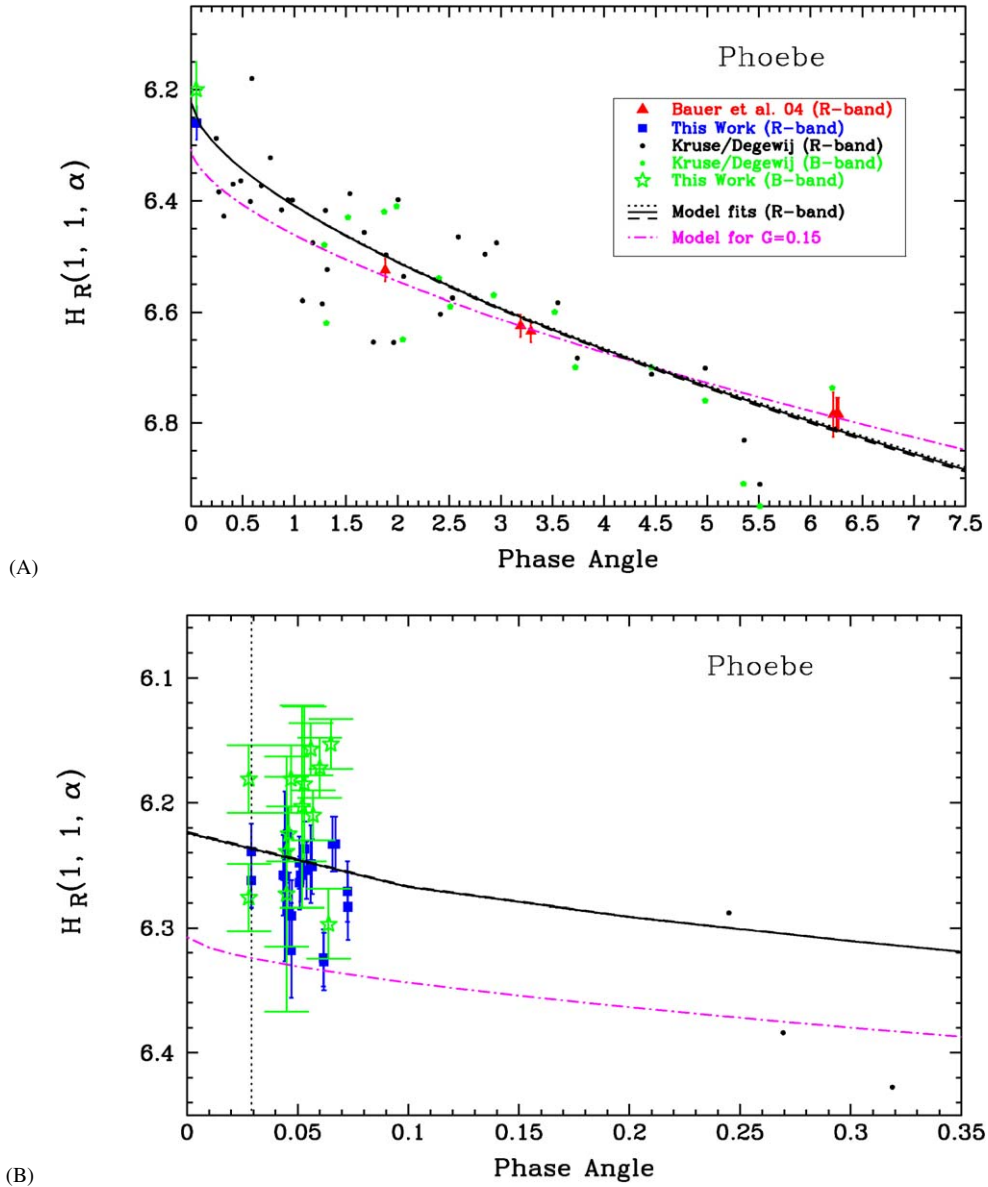


Fig. 1. Phoebe’s phase curve data. Panel A shows the data points from the literature, including the R-band data from Bauer et al. (2004) (red, or gray, triangles), the B-band (green, or gray, dots) and R-band (black dots) from Kruse et al. (1986) and Degewij et al. (1980), and the average R-band (blue, or dark, square) and B-band (green, or light, star) from Saturn’s 2005 opposition. The B-band points are offset to align with the R-band data using B–R colors from Degewij et al. (1980). The lines indicate the IAU 2-parameter model fits to the R-band data. The magenta (or gray) dot-dash line is for a previous fit to the Bauer et al. (2004) data yielding a slope parameter G of 0.15. The black solid line indicates our best fit including our 2004 data and the R-band 2005 average, while the dotted and dashed lines indicate the limits of the errors (see Table 4). Panel B shows a close up of the opposition surge’s 2005 R- and B-band data points with the rotational light curve amplitude removed. The vertical dotted line indicates the Sun’s angular radius. Note the offset of the B band indicating a possibly stronger opposition surge in the B band.

ages, or if so, what the formal uncertainty was in the reported values. The uncertainty in the other photometry points from the literature were on the order of the dispersion we found in our 2005 opposition data set. The data reveal a shallow phase-curve with fit parameters similar to those of Albiorix. No B-band data were available for Tarvos, but the B-band opposition surge data for Albiorix show only a slightly brighter offset at the narrowest of angles, well below a $3\text{-}\sigma$ significance level. As in Figs. 1, 4, 6, and 7, the model fits shown were made for the R-band data, with the best fit model indicated by the solid lines and fit uncertainties by dashed and dotted lines. For both satellites, the

opposition surge was well-fit by the overall phase curve model derived from the entire data set.

3.1.3. Siarnaq

Siarnaq’s phase curve is shown in Fig. 4A, and our opposition surge data points are plotted in Fig. 4B. Siarnaq was reported by Buratti et al. (2005a) to show rotational brightness variations on the order of 6 h or more and an amplitude $\sim 0.05m_R$, smaller than the phase brightening effects we report here. Our data were consistent with a rotational light curve period of similar nature, but we were unable to place further

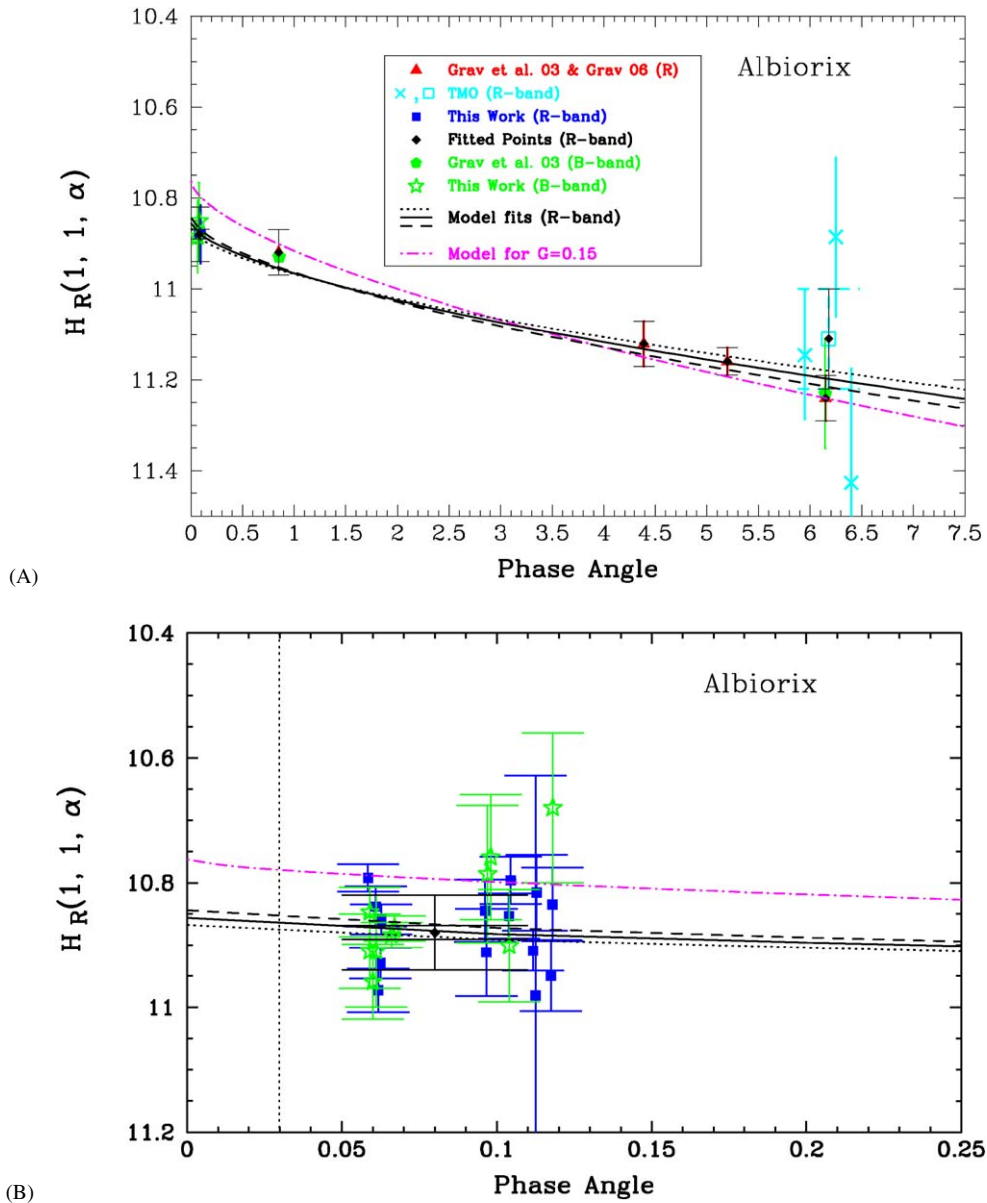


Fig. 2. The phase curve of Albiorix. Panel A shows the higher phase magnitudes, including the R-band data (red, or gray, triangles) and B-band (green, or gray, pentagons) from Grav et al. (2003) and Grav (2006; in preparation), and the TMO 0.6-m R-band values (cyan, or light gray, \times s) along with their average value (cyan, or light gray, open circle). The B-band values in the graph have been offset to align with the R-band magnitudes using the B–R colors from Grav et al. (2003). The average R-band (blue, or dark gray, square) and B-band (green, or gray, star) magnitudes from Saturn’s 2005 opposition are also shown. The black diamond overlays indicate which points were used for the model fits. As in Fig. 1, the black lines indicate the IAU 2-parameter model fits to the data (see Table 4) with the solid line indicating the best fit and the dot and dashed lines the fit’s $1-\sigma$ uncertainty extrema. The magenta dot-dashed line, included for comparison, is for a model with slope parameter G of 0.15. Panel B shows a close up of the opposition surge’s 2005 individual R- (blue square) and B-band (green star) magnitudes. The black diamond data point is the R-band average magnitude shown for comparison. The vertical dotted line indicates the Sun’s angular radius. Unlike Phoebe, there appears to be no significant offset between the B- and R-band opposition points. The two sets of error bars on the opposition surge magnitude averages are based on the dispersion of the points (larger value) and the statistically propagated errors (smaller value), which necessarily assumes no true significant intrinsic variation in the magnitudes over our sample.

meaningful constraints on the light curve characteristics. The higher phase angle magnitude values yield extremely shallow phase curve fits, uniquely so, and of the order of bright icy bodies, such as the satellite Europa or planet Pluto. Indeed, our model seems of limited use in this instance, as Siarnaq’s opposition surge portion of the curve appears too steep to fit with an IAU-type function. The steepnesses of the B- and R-band opposition surges appear to be similar, within the uncertainties, but

the magnitude of the narrow ($<1^\circ$) opposition surge appears to be comparable or greater than that of Phoebe’s. We used Grav (2006; in preparation) and TMO data points, and the discovery data points in our R-band model fits. The B-band data for Siarnaq was also fit with an IAU model, and the results are tabulated in Table 4. The B-band data fit yielded slightly steeper slope parameters when compared to the R-band fits, but not significantly different.

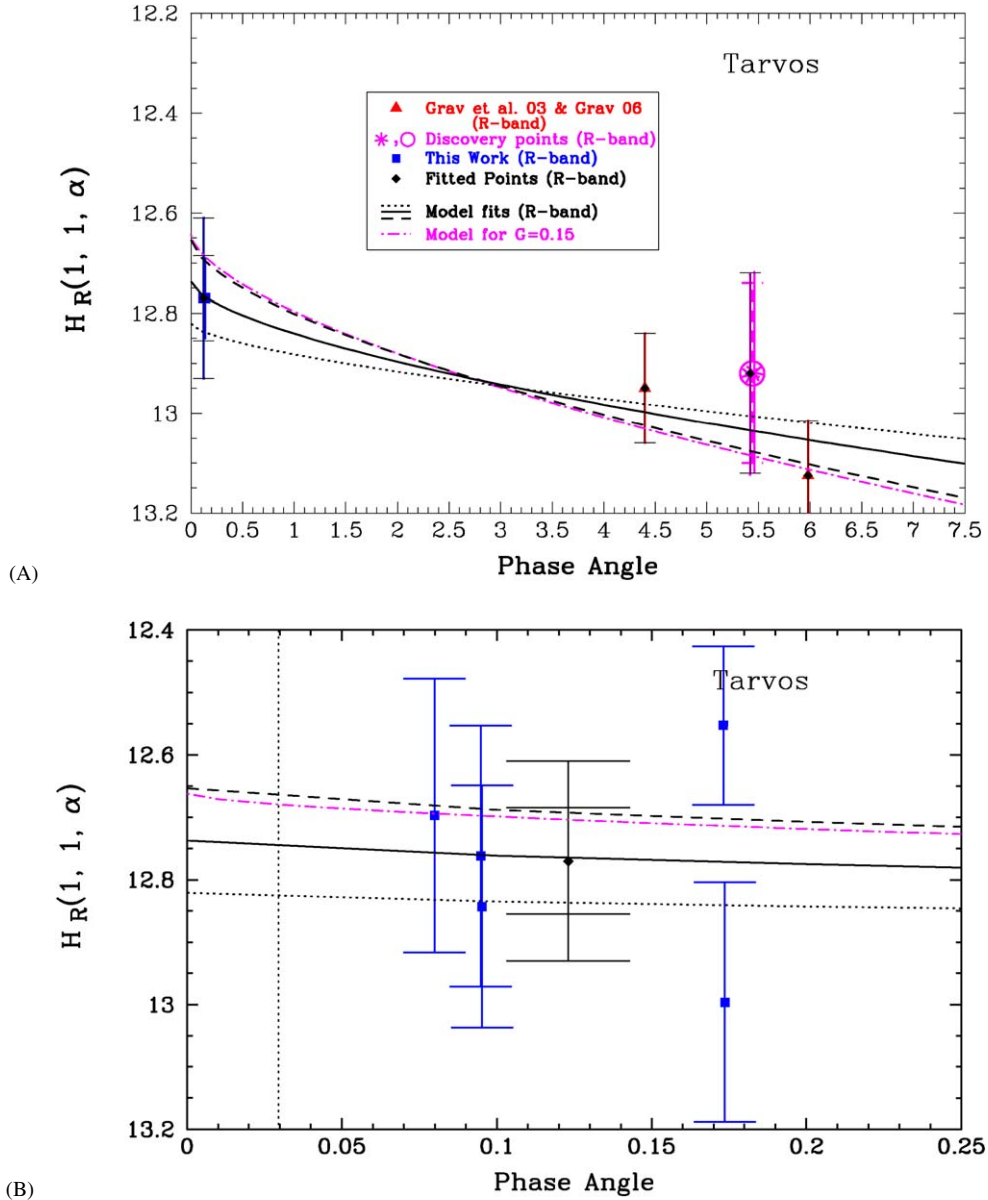


Fig. 3. The phase curve of Tarvos. Panel A shows the higher phase magnitudes, including the R-band data (red triangles) from Grav et al. (2003) and Grav (2006; in preparation). The average R band (blue square) from Saturn's 2005 opposition and the discovery data set (magenta asterisks; Gladman et al., 2000a) and its average (magenta open circle) are also shown. The black diamond overlays indicate which points were used for the fits. As in Fig. 2, the black lines indicate the IAU 2-parameter model fits to the data (see Table 4) with the solid line indicating the best fit and the dot and dashed lines the fit's $1-\sigma$ uncertainty extrema. A model with slope parameter G of 0.15 is included for comparison (magenta dot-dashed line). Panel B shows a close up of the opposition surge's 2005 R-band data points, and no rotational light curve was discernable from our points shown here. The vertical dotted line indicates the Sun's angular radius.

3.1.4. Ymir, Paaliaq, and Ijiraq

Recent work by Grav (2006; in preparation) suggests a higher than expected light curve amplitude for the satellite Ymir (amplitude $\sim 0.2m_R$). Only R-band data were available for the opposition data set. Ymir is the only satellite in our data set, with the possible near-exception of Phoebe, for which our data cover the true opposition signal, i.e., when the phase angle is considerably less than the solar angular radius. However, only three observation points were successfully made of Ymir, two of which were made only 7 min apart. Hence, the average of these three points may not be representative of the true light curve average, and we do not attempt to

fit a phase curve (Fig. 5). For Paaliaq, the R-band fit appears poorer by eye (Fig. 6), especially at higher phase angle samplings. However, our multiple opposition photometry points taken in January 2005 likely have sampled the range of the rotational variation, and the data point at $\alpha = 5.3^\circ$ from Grav (2006; in preparation) was derived from multiple points which similarly sampled the light curve's range (amplitude $\sim 0.1m_R$). It is clear that a fairly steep slope parameter value ($G \leq 0.15$) fits best, and this satellite's phase curve is reminiscent of some centaur phase curves (e.g., Bauer et al., 2002; Rousselot et al., 2005). B-band data were fit with the IAU model as well, and yielded steeper results (lower G -parameter values)

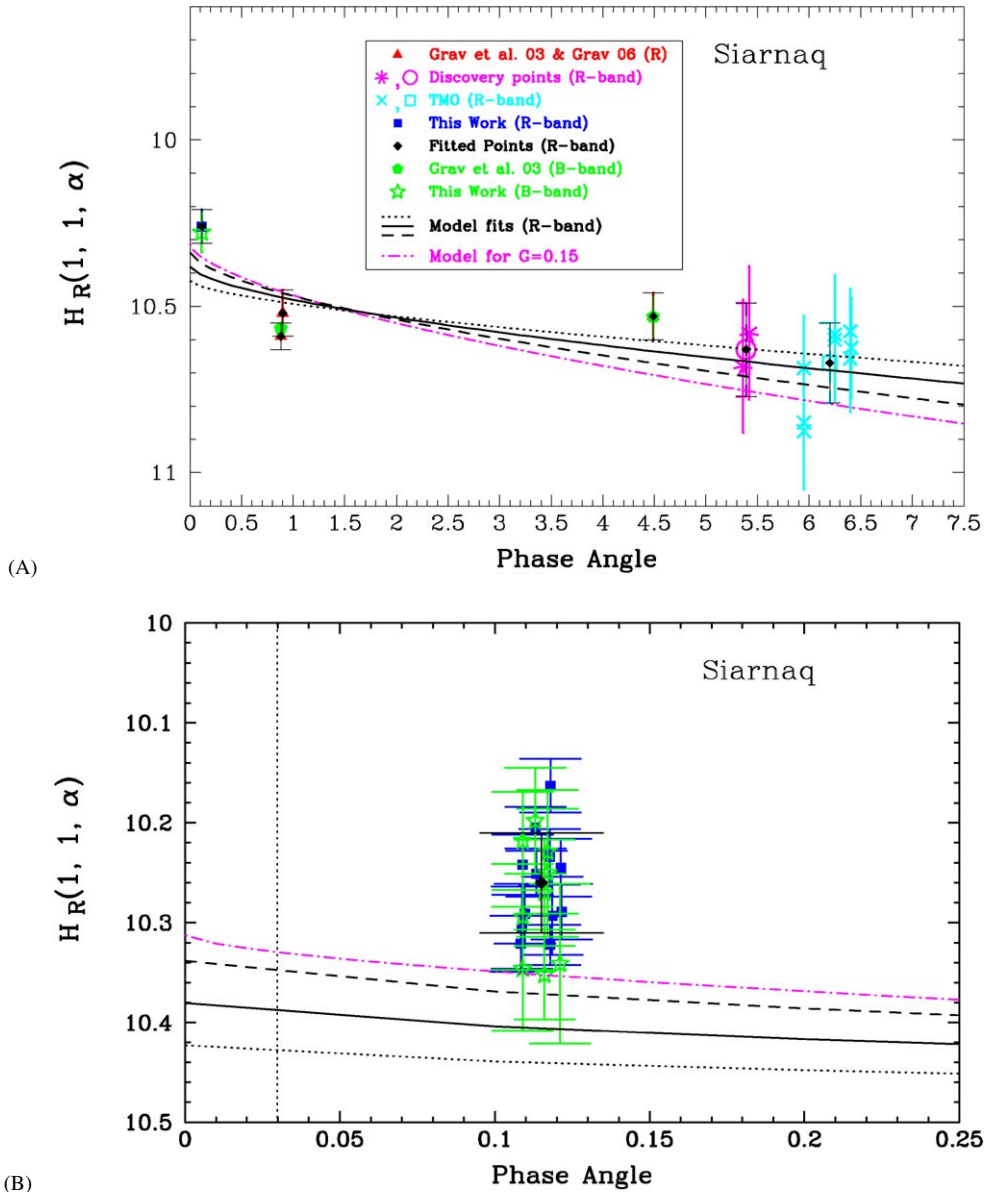


Fig. 4. The phase curve of Siarnaq. Panel A shows the higher phase magnitudes, including the R-band data (red triangles) and B-band (green pentagons) from Grav et al. (2003) and Grav (2006; in preparation), the discovery data points (magenta asterisks; Gladman et al., 2000a) and average (magenta open circle) and the TMO 0.6-m R-band (cyan- \times s) values along with their average value (cyan open square). The B-band values in the graph have been offset using the B–R colors from Grav et al. (2003). The average R band (blue square) and B band (green star) from Saturn’s 2005 opposition are also shown. The black diamond overlays indicate which points were used for the model fits. As in Fig. 1, the black lines indicate the IAU 2-parameter model fits to the data (see Table 4) with the solid line indicating the best fit and the dot and dashed lines the fit’s 1- σ uncertainty extrema. The magenta dot-dashed line, included for comparison, is for a model with slope parameter G of 0.15. Panel B shows a close up of the opposition surge’s 2005 R- and B-band data points similar to that in Fig. 2. The vertical dotted line indicates the Sun’s angular radius. Unlike Phoebe, there appears to be no significant offset between the B- and R-band opposition points.

to the R-band fit, but this does not include the multiply-sampled data values at 5.3° from Grav (2006; in preparation) which were provided only in the R band, and the statistical uncertainty overlaps the slope-parameter fit for the R band. The B-band data points in Fig. 6 are offset to align with the R band using the Grav et al. (2003) colors, as with Albiorix and Siarnaq. The B- and R-band opposition surges nearly match. In the case of Paaliaq, the opposition surge is still slightly steeper than what the IAU models predict.

The data for the satellite Ijiraq (R band only; Figs. 7A and 7B) again provided a steep phase curve fit. However, the un-

certainties in the magnitude values, ~ 0.2 , are fairly large, and the large range in the three opposition surge sample points may be caused in part by a large rotational light curve amplitude, although the S/N of our data are too low to constrain this possibility.

3.2. B–R colors and peak $H_R(1, 1, \alpha)$

The Palomar and CTIO colors and peak R band magnitude values are summarized in Table 5.

These are the values measured for $\alpha \approx \alpha_{\min}$, where $\alpha_{\min} \leq \alpha_R$ only for Phoebe and Ymir, and $\alpha \leq 0.1^\circ$ for the remain-

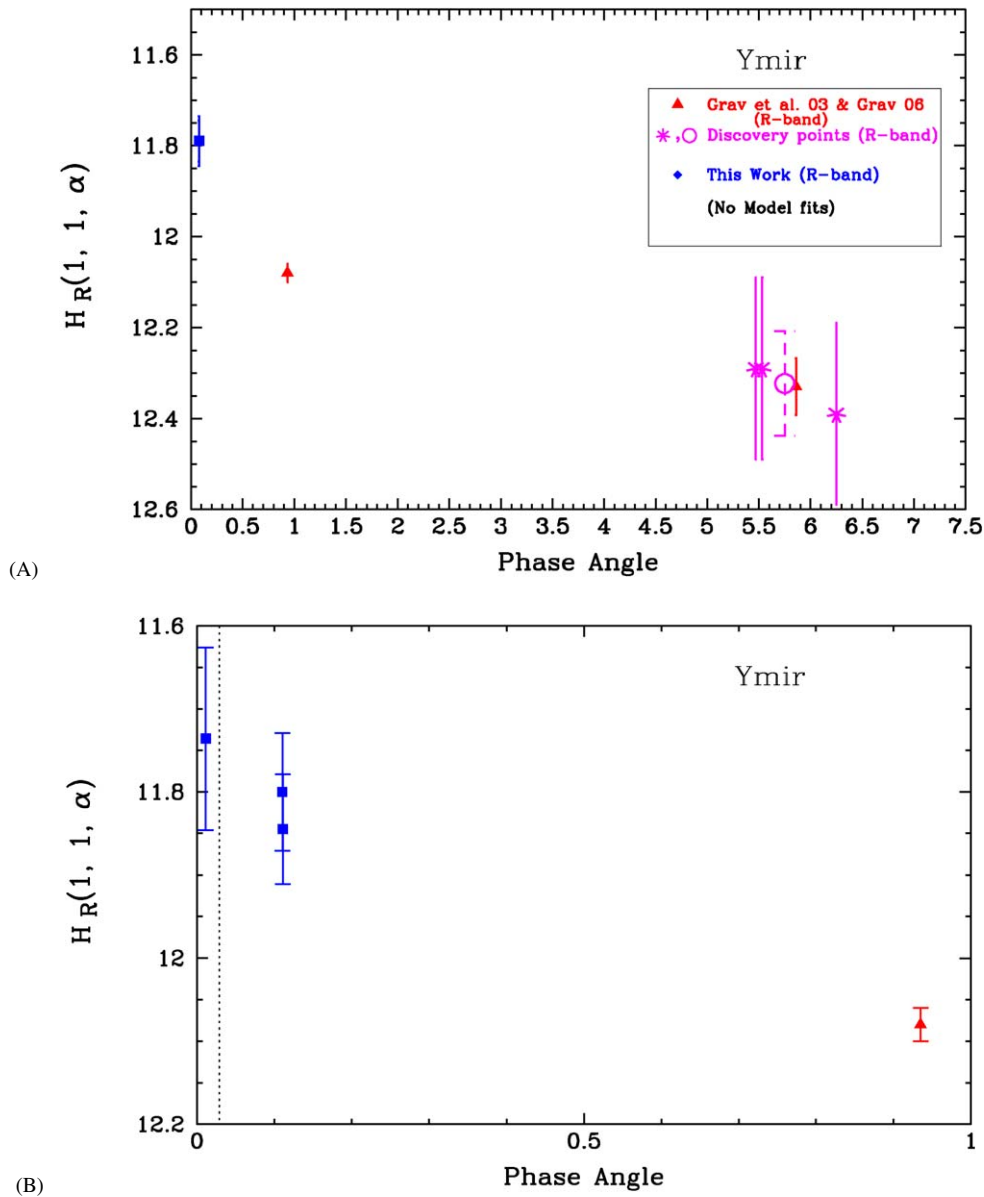


Fig. 5. The phase data points of Ymir. Panel A shows the higher phase magnitudes, including the R-band data (red triangles) from [Grav et al. \(2003\)](#) and Grav (2006; in preparation), and the R-band discovery points from [Gladman et al. \(2000b\)](#) (magenta asterisks, assuming a 0.2 magnitude uncertainty) along with their average value (magenta open circle). The average R band (blue square) from Saturn's 2005 opposition is also shown. No phase curve fits were attempted, owing to Ymir's reportedly large rotational light curve amplitude Grav (2006; in preparation). Panel B shows a close up of the opposition 2005 R-band data points. A possible ($<1\text{-}\sigma$ significance) brightening may have been detected in lowest phase angle point. The vertical dotted line indicates the Sun's angular radius.

ing satellites in our sample. Our color measurements of the [Gladman et al. \(2001\)](#) satellites agree with [Grav et al. \(2003\)](#) within the limits of our statistical uncertainty. However, at opposition, Phoebe appeared brighter in B than predicted by either [Grav et al. \(2003\)](#) or other sources in the literature (e.g., [Degewij et al., 1980](#) and [Kruse et al., 1986](#)), yielding a B–R value for our opposition magnitudes which is lower than expected.

4. Discussion

These data represent a unique set of photometric observations of outer Solar System objects. Not only are they the first observations of the phase curves opposition surges of the

[Gladman et al. \(2001\)](#) satellites, they provide some of the narrowest phase angle observations reported to date. The observations took place at unique geometries for an outer Solar System body in that in two cases the phase angle was less than the radius subtended by the solar disk at the satellite's heliocentric distance. At these angles, it may be expected that the opposition surge would begin to plateau in brightness, as the rays from opposite sides of the solar disk intercept the satellite's surface at different incident angles. This plateau should have been reached for Phoebe and Ymir, although for Phoebe, the effects of solar limb darkening may have diminished the finite-solar-disk effect by a few percent at its sampled phase angle. Except for possibly Ymir's smallest phase angle point, and a possible

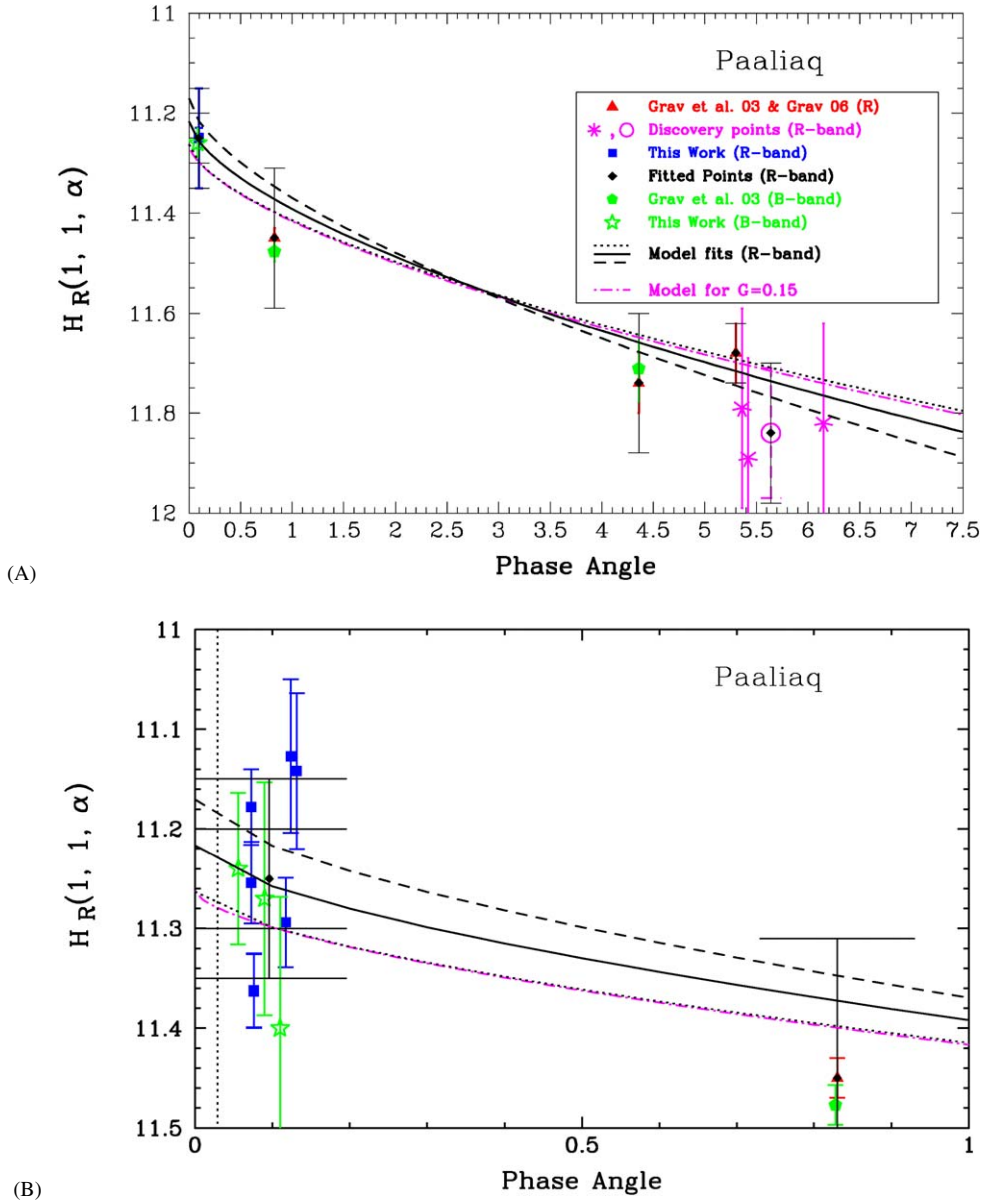


Fig. 6. The phase curve of Paaliaq. Panel A shows the higher phase magnitudes, including the R-band data (red triangles) and B-band (green pentagons) from Grav et al. (2003) and Grav (2006; in preparation), and the discovery data points (magenta asterisks) and average (magenta open circle; Gladman et al., 2000b). The B-band values in the graph have been offset using the B–R colors from Grav et al. (2003). The average R band (blue square) and B band (green star) from Saturn’s 2005 opposition are also shown. The black diamond overlays indicate which points were used for the model fits. As in Fig. 1, the black lines indicate the IAU 2-parameter model fits to the data (see Table 4) with the solid line indicating the best fit and the dot and dashed lines the fit’s $1\text{-}\sigma$ uncertainty extrema. The magenta dot-dashed line, included for comparison, is for a model with slope parameter G of 0.15. Panel B shows a close up of the opposition surge’s 2005 R- and B-band data points. The vertical dotted line indicates the Sun’s angular radius. Unlike Phoebe, there appears to be no significant offset between the B- and R-band opposition points.

subtle brightening trend for Phoebe’s opposition surge magnitudes, little difference can be seen between the opposition surge behavior when the phase angle became less than the solar disk size and when it was larger, out to $\alpha \approx 0.1^\circ$. Statistically, these narrowest angle brightenings for Phoebe and Ymir are not significant differences in the magnitudes, especially in the case of Ymir, which does not have its rotation light curve adequately sampled here, and may have a large light curve amplitude (Grav, 2006; in preparation).

Starting with the most well characterized satellite, we note that Phoebe’s phase curve shows a considerably steep slope. At visual wavelengths, Phoebe appears to have a C-type spectrum

(Buratti et al., 2002), and resolved measurements by spacecraft observations yield albedo estimates that would place Phoebe at the brighter end of the C-type asteroids. The near-infrared spectrum (1 to 5 μm) of the non-ice region of Phoebe, however, matches that of the dark side of Iapetus (Buratti et al., 2005b), and Phoebe’s unique environment is potentially more collisionally active relative to the asteroid main belt and may explain its battered appearance (e.g., Neukum et al., 2005); the C-type analogy may not be universally rigorous. Over the entire phase curve sampled here, the IAU model fit to the data yields a value of $G = +0.02 \pm 0.03$, comparable to the extreme end of the darkest C- or D-type asteroids and perhaps more appropriately

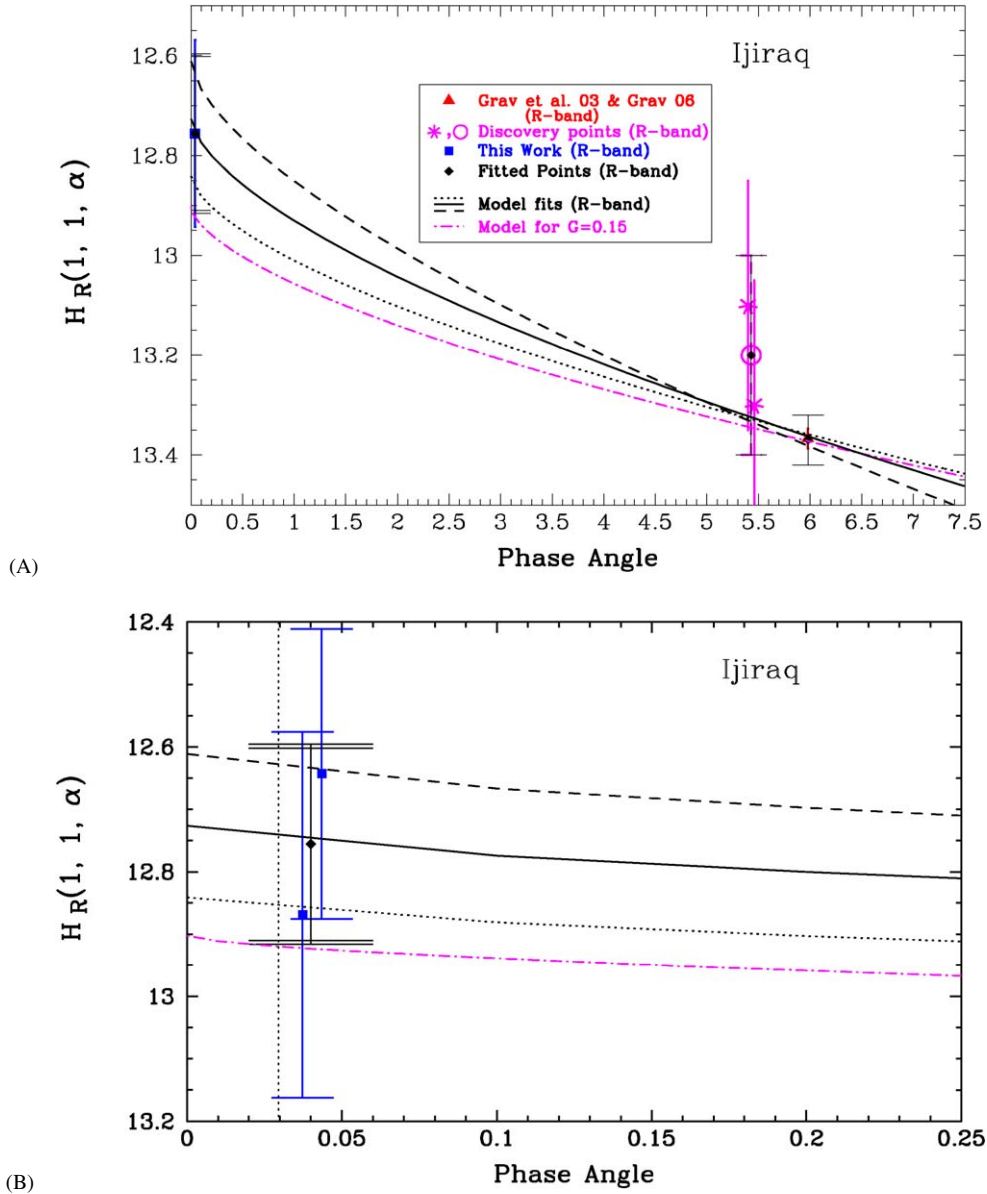


Fig. 7. The phase curve of Ijiraq. Panel A shows the higher phase magnitudes, including the R-band data (red triangles) from Grav et al. (2003) and Grav (2006; in preparation), and the R-band discovery points from Gladman et al. (2000c) (magenta asterisks, assuming a 0.25 magnitude uncertainty) values along with their average value (magenta open circle). The dispersion in the individual magnitude measurements was folded into the reported uncertainties of the averages. The average R band (blue square) from Saturn's 2005 opposition is also shown. The black diamond overlays indicate which points were used for the fits. As in Fig. 1, the black lines indicate the IAU 2-parameter model fits to the data (see Table 4) with the solid line indicating the best fit and the dot and dashed lines the fit's 1σ uncertainty extrema. A model with slope parameter G of 0.15 is included for comparison (magenta dot-dashed line). Panel B shows a close up of the opposition surge's 2005 R-band data points, and no rotational light curve was discernable from our points shown here. The vertical dotted line indicates the Sun's angular radius.

very near the mean of reported centaur phase curves (~ 0.01 considering Bauer et al., 2003 and Rousselot et al., 2005). An identical method was applied to points excluding the opposition surge by Bauer et al. (2004), and earlier by Kruse et al. (1986), and yielded similar G -parameters near 0.15, consistent with mid-range C- and D-type asteroids and some centaur phase curves. Hence, the sampling of the opposition surge significantly changed the fit. In considering which is a better fit overall, Simonelli et al. (1999) conducted Hapke model fits to the Voyager data set with more extensive coverage at higher phase angles, and adopted a phase integral value, q , on the or-

der of 0.24, which would roughly correspond to a G -parameter near or less than 0, while a $G = 0.15$ would yield a $q \approx 0.39$ (Bowell et al., 1989).

In consideration of cross comparisons among these irregular satellites, one group stands out. Table 4 shows the phase curve 2-parameter IAU model fit results, including the fit slope parameter values, G , and peak 0° phase angle brightness, $H_R(1, 1, 0)$. The fits were made using the R band magnitudes, since these spanned the largest phase angle coverage among the data sets. The satellites we sampled from the 34° inclination ($i = 34^\circ$) group, Albiorix and Tarvos, have comparatively

Table 5
Measured colors and $H_R(1, 1, 0)$

Object	$H_R(1, 1, 0)$	σ_H	B–R	σ_{B-R}
Phoebe	6.26	0.03	0.95	0.06
Albiorix	10.87	0.06	1.32	0.08
Tarvos	12.77	0.16	–	–
Siarnaq	10.28	0.05	1.31	0.04
Paaliaq	11.24	0.10	1.30	0.20
Ymir	11.89	0.12	–	–
Ijiraq	12.75	0.15	–	–
<i>Solar</i>	–	–	1.01	0.03

shallow phase curves and muted opposition surge peaks. Slope parameters of ~ 0.4 fit the measurements for both satellites reasonably well (within the $1\text{-}\sigma$ uncertainty), including the opposition surge points. These are the only satellites we sampled where this is the case. Most others (all but one; Siarnaq) show significantly steeper phase curve slopes across the phase angles sampled, and all show stronger opposition surges. This phase curve analysis has independently identified these satellites as a potentially special group, with slope parameter values similar to moderate-albedo asteroids, such as S-, Q- or M-type (Bowell et al., 1989). The cause of the surge suppression may be a higher surface compaction state. In any event, the observation serves as further evidence that the bodies of the $i = 34^\circ$ dynamical class are related in origin as well as unique from the other irregulars.

Cuk and Burns (2004) identified the Albiorix group (“Gaulish cluster”) as being “non-main-sequence” irregulars, suggesting a unique origin apart from the other newly discovered irregulars. Their shared phase curve shapes may serve as further evidence for their shared and distinct origin. Although they possess similar inclinations ($i \approx 46^\circ$), Siarnaq, Paaliaq, and Ijiraq all seem to inhabit different dynamical groupings associated with resonances (Cuk and Burns, 2004). Hence, one may not expect that they necessarily have a common origin, as Tarvos and Albiorix might. Our phase curve observations generally support this possibility. The difference in the phase curve fits from this group show different slope parameters, ranging from G_R values of -0.11 to $+0.45$.

Siarnaq’s phase curve is nearly flat, and shallower at higher phase angles than any of the others. Our IAU model fits for this satellite show the largest slope parameter of our sampled objects ($G = 0.45 \pm 0.17$), on the highest end of the typical range of main belt asteroids ($G \sim 0.1$ to 0.5 ; Bowell et al., 1989), similar to an E-, R- or V-type. The steep opposition surge, ~ 0.2 magnitudes for $\alpha \leq 0.8^\circ$, is not altogether different from those observed on other outer Solar System satellites. Europa, for example, has a fairly weak phase curve slope until angles of $\alpha < 1^\circ$ (Helfenstein et al., 1998) while Hapke modeling predicted a higher porosity (Domingue and Verbiscer, 1997) among the smaller particles. The same may be said for the uranian satellite Oberon, a comparatively darker object, but with a similar phase curve brightening for $\alpha < 1^\circ$ (Helfenstein et al., 1991). The behavior of Siarnaq’s phase curve, steep for phase angles short-ward of 0.8° , and shallow at phase angles long-ward of 0.8° , is unique among our sample of satellites. Siarnaq is the largest (or at least the brightest) of the new irregu-

lar satellites, and so could have maintained the most substantial regolith.

The remaining irregular satellites in our sample show considerably steeper phase curves, with more prominent opposition surges. Paaliaq shows a steep phase curve, with a fitted phase curve slope parameter near zero. Ijiraq, with a similar inclination as Siarnaq, has the apparently steepest slope fit, but our data have admittedly poorer S/N for this object, and only three phase angles sampled and two photometry points at opposition. Still, even with the slope parameter’s uncertainty, Ijiraq’s phase curve steepness is at least near the centaur mean, as opposed to within the range of most main belt asteroids. Indeed, phase curve fits for these two satellites, which yield slope parameter values spanning $+0.04$ to -0.13 , are similar to those of the centaurs (e.g., Bauer et al., 2003 and Rousselot et al., 2005); this may be indicative of similar origin between these irregulars and the centaur population.

Many outer Solar System bodies have phase curves that have steep G parameters when fit to the IAU model, and it is worth testing whether the observed opposition surge is an effect of being able to sample the body’s opposition surge down to narrower angles since these objects reside at greater heliocentric distances. This may indicate that the steeper surges are caused by the sampling effects, or possibly the angular size of the solar disk, which may allow for narrower angles at which the plateau effect, described earlier, may take place. Fig. 8 shows the steepness of the opposition surges, the brightening between $2^\circ < \alpha < 0.1^\circ$, as a function of distance from the Sun, and no such correlation is apparent in the literature sampled. Hence, the phase curve steepness, even at narrow angles, is likely indicative of the physical nature of the surface, rather than an artifact of the sampling or an optical phenomenon related to solar distance alone.

What the surface characteristic may be, whether it is a CBS or particle compactness phenomenon, may not be obvious, especially as our narrowest phase angle points are somewhat isolated relative to the next highest phase angle points, and lie in a regime where both effects may be strong (Hapke, 1993). However, Phoebe’s phase curve may provide some useful information applicable to this problem. There is apparent in all the satellites an anti-correlation with the strength of the opposition surge and increasing wavelength. Like all of our model fits to the irregular satellites with both B- and R-band data, Phoebe’s slope parameter is steeper in the B band than in the R band (see Table 4), but Phoebe’s is unique in that the uncertainties are small and the offset in G values between the R- and B-band data sets are significantly different. CBS, a multiple-scattering effect, has been shown to be strongest on surfaces with moderate reflectivity (e.g., Domingue et al., 2002 and Nelson et al., 2000), and at longer wavelengths (Hapke, 1993). Steeper phase curves relating to particle–particle shading, a single-scattering effect, are strongest with lower reflectance surfaces (Shkuratov and Helfenstein, 2001). As Phoebe has a relatively neutral to slightly red spectral reflectance (Buratti et al., 2002), and a full-disk albedo in the V band ~ 0.08 , less than 0.15 (Simonelli et al., 1999) a brighter surge in the B band, as observed, may indicate a mostly particle-shading ef-

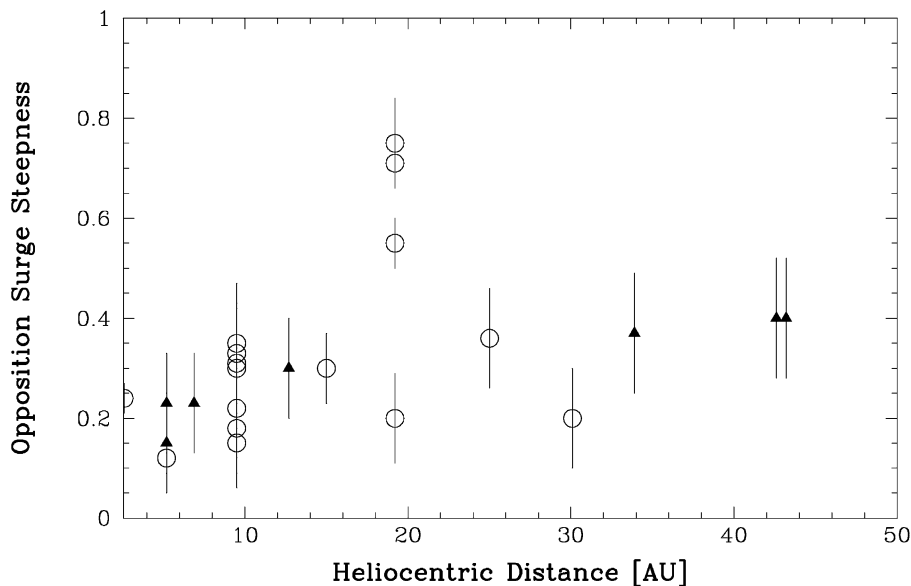


Fig. 8. The opposition surge steepness as a function of solar distance. The surge steepness was measured as the magnitude difference between 2° and 0.1° phase angle brightness. Phase curves from this work (9.5 AU), Bauer et al. (2003) (Hylonome; 25 AU), Buratti et al. (1990) (uranian satellites; 19.2 AU), Johnson (1971) (Galilean satellites; 5.2 AU), Delahodde et al. (2001) (28P/Neujmin 1; 6.9 AU), Sheppard and Jewitt (2002) (1999 DE9; 33.9 AU), Hicks et al. (2005) (Varuna; 43.2 AU), Verbiscer et al. (2005b) (Enceladus; 9.5 AU), Shevchenko et al. (2002) and Belskaya and Shevchenko (2000) (F-type main belt asteroids; 2.6 AU), Rousselot et al. (2005) (2002 UX25; 42.6 AU), Rousselot et al. (2003) (1999 TD10; 12.7 AU), and Herbert et al. (2004) (Triton; 30.1 AU) were included in the plot. The data were selected for phase coverage spanning at least 0.2° to 1.2° . Data spanning 0.1° through 2° are marked with open circles. If extrapolations were necessary out to 0.1° or 2° , the magnitudes are marked with filled triangles. The KBOs were extrapolated outward to 2° from $\sim 1.5^\circ$ for 1999 DE9 and from $\sim 1.2^\circ$ for Varuna and 2002 UX25. Note there is no separate grouping between regular and irregular satellites for Saturn in our sample. Enceladus is mixed in with Albiorix and Tarvos (with their opposition surge magnitudes clustered around 0.2), and Phoebe with the remainder in our sample (clustered around 0.35). The opposition surge groupings of the irregular satellites as charted here qualitatively match the G -parameter values, with the exception of Siarnaq, which has a shallow phase curve at larger angles, but a strong opposition surge (see Fig. 4A).

fect. The geometry of ground based observing limits the data to a small span of phase angles. Phoebe alone is the satellite in our sample that has been explored by spacecraft (Simonelli et al., 1999, 2004). Bodies with potentially comparable physical nature, such as KBOs and Pluto, will be explored in the future by missions such as New Horizons, and data of the kind reported here will be crucial to the interpretation of the data they obtain.

5. Conclusions

Our study of Saturn's irregular satellites during the opposition of 2005 provided us with a rare opportunity to characterize their phase curves and opposition surges. The brightnesses obtained were for phase angles that were not only uniquely low for the objects we observed, but also for any objects at these solar distances. We found:

- With three notable exceptions, the irregular satellites have similar phase curve and opposition surge behavior to many of the centaurs.
- Albiorix and Tarvos come from the $i \approx 34^\circ$ dynamical group, and both show uniquely shallow phase curves and muted opposition surges that support a common origin for this dynamical classification's members.
- Siarnaq shows a strong opposition surge with an otherwise shallow phase curve slope, similar to Europa's and

Oberon's phase curve behavior, which have been interpreted as indicating higher porosity or particle compaction at smaller particle scales.

- The differences in phase curve shapes among the $i \approx 46^\circ$ group members indicate a clustering more consistent with Cuk and Burns' (2004) interpretation of the group's origin.
- Phoebe's phase curve steepens with the inclusion our 2005 opposition data set. Phoebe's B-band opposition surge is stronger than its R band, arguing against a CBS dominant effect at narrow phase angles.
- There is no evidence for a relation with observed opposition surge steepness based solely upon heliocentric distance.
- Phase curve measurement and analysis is a useful tool in seeking or testing interrelationships among small bodies. These data suggest, but do not conclusively prove, a correlation between the dynamical classification of the irregular satellites and their phase curve shapes.

Acknowledgments

The authors thank the personnel of Palomar Observatory, CTIO, and TMO, and in particular Rick Burruss and Jeff Hickey. J. Bauer gratefully acknowledges the support of the NRC postdoctoral fellowship program during the time the data were collected, and the NASA Planetary Astronomy research program.

References

- Bauer, J.M., Meech, K.J., Fernández, Y.R., Farnham, T.L., Roush, T.L., 2002. Observations of the Centaur 1999 UG5: Evidence of a unique outer Solar System surface. *Publ. Astron. Soc. Pacific* 114, 1309–1321.
- Bauer, J.M., Meech, K.J., Fernández, Y.R., Pittichova, J., Hainaut, O.R., Boehnhardt, H., Delsanti, A.C., 2003. Physical survey of 24 centaurs with visible photometry. *Icarus* 166, 195–211.
- Bauer, J.M., Buratti, B.J., Simonelli, D.P., Owen, W.M., 2004. Recovering the rotational light curve of Phoebe. *Astrophys. J.* 610, L57–L60.
- Belskaya, I.N., Shevchenko, V.G., 2000. Opposition effect of asteroids. *Icarus* 147, 94–105.
- Bowell, E., Hapke, B., Domingue, D., Lumme, K., Peltoniemi, J., Harris, A.W., 1989. Application of photometric models to asteroids. In: Binzel, R.P., Gehrels, T., Matthews, M.S. (Eds.), *Asteroids II*. Univ. of Arizona Press, Tucson, pp. 524–556.
- Brown, M.E., 2000. Near-infrared spectroscopy of centaurs and irregular satellites. *Astron. J.* 119, 977–983.
- Buratti, B.J., Veverka, J., 1985. Photometry of rough planetary surfaces—The role of multiple scattering. *Icarus* 64, 320–328.
- Buratti, B., Wong, F., Mosher, J., 1990. Surface properties and photometry of the uranian satellites. *Icarus* 84, 203–214.
- Buratti, B.J., Hillier, J.K., Wang, M., 1996. The lunar opposition surge: Observations by Clementine. *Icarus* 124, 490–499.
- Buratti, B.J., Hicks, M.D., Tryka, K.A., Sittig, M.S., Newburn, R.L., 2002. High resolution 0.33–0.92 μm spectra of Iapetus, Hyperion, Phoebe, Rhea, Dione, and D-type asteroids: How are they related? *Icarus* 155, 375–381.
- Buratti, B.J., Hicks, M.D., Davies, A., 2005a. Spectrophotometry of the small satellites of Saturn and their relationship to Iapetus, Phoebe, and Hyperion. *Icarus* 175, 490–495.
- Buratti, B.J., and 28 colleagues, 2005b. Cassini Visual and Infrared Mapping Spectrometer observations of Iapetus: Detection of CO₂. *Astrophys. J.* 622, L149–L152.
- Clark, R.N., and 25 colleagues, 2005. Compositional maps of Saturn's moon Phoebe from imaging spectroscopy. *Nature* 435, 66–69.
- Cuk, M., Burns, J.A., 2004. On the secular behavior of irregular satellites. *Astron. J.* 128, 2518–2541.
- Degewij, J., Zellner, B., Andersson, L.E., 1980. Photometric properties of outer planetary satellites. *Icarus* 44, 520–540.
- Delahodde, C.E., Meech, K.J., Hainaut, O.R., Dotto, E., 2001. Detailed phase function of Comet 28P/Neujmin 1. *Astron. Astrophys.* 376, 672–685.
- Domingue, D., Verbiscer, A., 1997. Re-analysis of the solar phase curves of the icy Galilean satellites. *Icarus* 128, 49–74.
- Domingue, D.L., Robinson, M., Carcich, B., Joseph, J., Thomas, P., Clark, B.E., 2002. Disk-integrated photometry of 433 Eros. *Icarus* 155, 205–219.
- Durda, D.D., Stern, S.A., 2000. Collision rates in the present-day Kuiper belt and centaur regions: Applications to surface activation and modification on comets, Kuiper belt objects, centaurs, and Pluto–Charon. *Icarus* 145, 220–229.
- Gladman, B., Holman, M., 2000. S/2000 S 11. *IAU Circ.* 7545, 4.
- Gladman, B., Kavelaars, J., Allen, R.L., Rigg, T., Hergenrother, C.W., Larson, S.M., Doressoundiram, A., Romon, J., 2000a. S/2000 S 3 and S/2000 S 4. *IAU Circ.* 7513, 1.
- Gladman, B., Kavelaars, J., Petit, J.M., Scholl, H., Holman, M., Marsden, B.G., Nicholson, P., Burns, J.A., 2000b. S/2000 S 1 and S/2000 S 2. *IAU Circ.* 7512, 1.
- Gladman, B., Gray, W.J., Marsden, B.G., 2000c. S/2000 S 5 and S/2000 S 6. *IAU Circ.* 7521, 1.
- Gladman, B., and 10 colleagues, 2001. Discovery of 12 satellites of Saturn exhibiting orbital clustering. *Nature* 412, 163–166.
- Grav, T., Holman, M.J., 2004. Near-infrared photometry of the irregular satellites of Jupiter and Saturn. *Astrophys. J.* 605, L141–L144.
- Grav, T., Holman, M.J., Gladman, B.J., Aksnes, K., 2003. Photometric survey of the irregular satellites. *Icarus* 166, 33–45.
- Hapke, B., 1993. *Theory of Reflectance and Emittance Spectroscopy*. Topics in Remote Sensing. Cambridge Univ. Press, Cambridge, UK.
- Hapke, B., 2002. Bidirectional reflectance spectroscopy. 5. The coherent backscatter opposition effect and anisotropic scattering. *Icarus* 157, 523–534.
- Helfenstein, P., Hillier, J., Weitz, C., Veverka, J., 1991. Oberon—Color photometry from Voyager and its geological implications. *Icarus* 90, 14–29.
- Helfenstein, P., Veverka, J., Hillier, J., 1997. The lunar opposition effect: A test of alternative models. *Icarus* 128, 2–14.
- Helfenstein, P., Currier, N., Clark, B.E., Veverka, J., Bell, M., Sullivan, R., Klemaszewski, J., Greeley, R., Pappalardo, R.T., Head, J.W., Jones, T., Klaasen, K., Magee, K., Geissler, P., Greenberg, R., McEwen, A., Phillips, C., Colvin, T., Davies, M., Denk, T., Neukum, G., Belton, M.J.S., 1998. Galileo observations of Europa's opposition effect. *Icarus* 135, 41–67.
- Herbert, B.D., Buratti, B.J., Schmidt, B., Bauer, J.M., Hicks, M.D., 2004. Observation of an opposition surge on Triton. In: *AAS/Division for Planetary Sciences Meeting Abstracts* 36. Abstract 17.10.
- Hicks, M.D., Simonelli, D.P., Buratti, B.J., 2005. Photometric behavior of 20000 Varuna at very small solar phase angles. *Icarus* 176, 492–498.
- Horner, J., Evans, N.W., Bailey, M.E., 2004. Simulations of the population of centaurs. I. The bulk statistics. *Mon. Not. R. Astron. Soc.* 354, 798–810.
- Irvine, W.M., 1965. The shadowing effect in diffuse reflection. *J. Geophys. Res.* 71, 2931–2937.
- Johnson, T.V., 1971. Galilean satellites: Narrowband photometry 0.30 to 1.10 μm . *Icarus* 14, 94–111.
- Johnson, T.V., Lunine, J.I., 2005. Saturn's moon Phoebe as a captured body from the outer Solar System. *Nature* 435, 69–71.
- Kruse, S., Klavetter, J.J., Dunham, E.W., 1986. Photometry of Phoebe. *Icarus* 68, 167–175.
- Landolt, A.U., 1992. UVRI photometric standard stars in the magnitude range 11.5–16.0 around the celestial equator. *Astron. J.* 104, 340–371.
- Luu, J., 1994. Comets disguised as asteroids. *Publ. Astron. Soc. Pacific* 106, 425–435.
- Nelson, R.M., Hapke, B.W., Smythe, W.D., Spilker, L.J., 2000. The opposition effect in simulated planetary regoliths. Reflectance and circular polarization ratio change at small phase angle. *Icarus* 147, 545–558.
- Neukum, G., Wagner, R.J., Denk, T., Porco, C.C., and the Cassini ISS Team, 2005. The cratering record of the saturnian satellites Phoebe, Tethys, Dione and Iapetus in comparison: First results from analysis of the Cassini ISS imaging data. *Lunar Planet. Sci.* 36. Abstract 2034.
- Oetking, P., 1966. Photometric studies of diffusely reflecting surfaces with applications to the brightness of the Moon. *J. Geophys. Res.* 71, 2505–2513.
- Owen, T.C., Cruikshank, D.P., Dalle Ore, C.M., Geballe, T.R., Roush, T.L., de Bergh, C., 1999. Note: Detection of water ice on Saturn's satellite Phoebe. *Icarus* 139, 379–382.
- Ozrin, V.D., 1992. Exact solution for coherent backscattering of polarized light from a random medium of random backscatterers. *Waves Random Med.* 2, 141–164.
- Pickering, W.H., 1899. A new satellite of Saturn. *Harvard College Observatory Circ.* 43, 1–3.
- Rousselot, P., Petit, J.M., Poulet, F., Lacerda, P., Ortiz, J., 2003. Photometry of the Kuiper-belt object 1999 TD₁₀ at different phase angles. *Astron. Astrophys.* 407, 1139–1147.
- Rousselot, P., Petit, J.M., Poulet, F., Sergeev, A., 2005. Photometric study of Centaur (60558) 2000 EC₉₈ and trans-neptunian object (55637) 2002 UX₂₅ at different phase angles. *Icarus* 176, 478–491.
- Seeliger, H., 1895. Theorie der Beleuchtung staubformiger kosmischen Massen insbesondere des Saturnringes. *Abhandlungen der Bayerischen Akademie der Wissenschaften, Mathematisch-Physikalische Klasse II* 18, 1–72.
- Sheppard, S.S., Jewitt, D.C., 2002. Time-resolved photometry of Kuiper belt objects: Rotations, shapes, and phase functions. *Astron. J.* 124, 1757–1775.
- Shevchenko, V.G., Belskaya, I.N., Krugly, Yu.N., Chiomy, V.G., Gaftonyuk, N.M., 2002. Asteroid observations at low phase angles. II. 5 Astraea, 75 Eurydike, 77 Frigga, 105 Artemis, 119 Althaea, 124 Alkeste, and 201 Penelope. *Icarus* 155, 365–374.
- Shkuratov, Y.G., Helfenstein, P., 2001. The opposition effect and the quasi-fractal structure of regolith. I. Theory. *Icarus* 152, 96–116.

- Simonelli, D.P., Kay, J., Adinolfi, D., Veverka, J., Thomas, P.C., Helfenstein, P., 1999. Phoebe: Albedo map and photometric properties. *Icarus* 138, 249–258.
- Simonelli, D.P., Buratti, B.J., Hicks, M.D., Brown, R.H., Clark, R.N., Cruikshank, D.P., Jaumann, R., McCord, T.B., Nelson, R.M., 2004. The roughness of Phoebe as determined by Cassini VIMS. In: AAS/Division for Planetary Sciences Meeting Abstracts 36. Abstract 04.03.
- Tholen, D.J., Tedesco, E.F., 1994. Pluto's lightcurve: Results from four oppositions. *Icarus* 108, 200–208.
- Tody, D., 1986. The IRAF data reduction and analysis system. In: Grawford, D.L. (Ed.), *Instrumentation in Astronomy VI*. In: Proc. SPIE, vol. 627. SPIE, Bellingham, WA, pp. 733–748.
- Verbiscer, A., French, R.G., Helfenstein, P., 2005a. Saturn's inner satellites at true opposition: Observations during a central transit of the Earth across the solar disk. In: AAS/Division for Planetary Sciences Meeting Abstracts 37. Abstract 36.05.
- Verbiscer, A.J., French, R.G., McGhee, C.A., 2005b. The opposition surge of Enceladus: HST observations 338–1022 nm. *Icarus* 173, 66–83.